Ann. Telecommun. (2011) 66:257–273
DOI 10.1007/s12243-010-0191-1

New super-orthogonal space-time trellis codes using differential *M*-PSK for noncoherent mobile communication systems with two transmit antennas

Corneliu Eugen D. Sterian · Yuanyuan Ma · Matthias Pätzold · Ion Bănică · Huaqiang He

Received: 9 March 2010 / Accepted: 2 July 2010 / Published online: 22 July 2010

Abstract In this paper, we develop super-orthogonal space-time trellis codes (SOSTTCs) using differential binary phase-shift keying, quadriphase-shift keying and eight-phase shift keying for noncoherent communication systems with two transmit antennas without channel state information at the receiver. Based on a differential encoding scheme proposed by Tarokh and Jafarkhani, we propose a new decoding algorithm with reduced decoding complexity. To evaluate the performance of the SOSTTCs by way of computer simulations, a geometric two-ring channel model is employed throughout. The simulation results show that the new decoding algorithm has the same decoding performance compared with the traditional decoding strategy, while it reduces significantly the overall computing complexity. As expected the system performance depends greatly on the antenna spacing and on the angular spread of the incoming waves. For fair comparison, we also design SOSTTCs for coherent detection of the same complexity as those demonstrated for the noncoherent case. As in the case of classical single antenna transmission systems, the coherent scheme outperforms the differential one by approximately 3 dB for SOSTTCs as well.

Keywords Differential detection · Noncoherent communications · Super-orthogonal space-time trellis codes

C. E. D. Sterian (✉) · I. Bănică
Polytechnic University of Bucharest, Splaiul Independentei 313 A, Bucharest 77206, Romania
e-mail: steriancorneliu@hotmail.com

I. Bănică
e-mail: ibanica@yahoo.com

Y. Ma · M. Pätzold · H. He
University of Agder, Televeien 9, 4879 Grimstad, Norway

Y. Ma
e-mail: yuanyuan.ma@uia.no

M. Pätzold
e-mail: matthias.paetzold@uia.no

H. He
e-mail: linzi_hust@163.com

1 Introduction

Space-time coding was introduced in the late 1990s as a promising technique to improve the reliability of mobile data links by using transmit antenna diversity [3, 20]. Those pioneering works and many others that soon followed were elaborated under the assumption that the receiver can acquire perfect *channel state information* (CSI). Nevertheless, the known-channel assumption may not be realistic in a scenario of rapidly changing fading environments. In our paper, we propose space-time trellis codes to be used in noncoherent transmission systems where neither the transmitter nor the receiver knows the fading gains of the channel. For the single-input single-output case, differential encoding coupled with trellis-coded modulation can provide a good solution to the problem [5, 13, 14, 23]. In the enlarged framework of multiple-input multiple-output (MIMO) systems, a new solution emerged as unitary space-time signals [2, 7–9]. Like Alamouti's scheme for coherent demodulation, these designs can provide diversity advantage, but no coding gain.

To obtain coding gains, trellis-coded unitary space-time modulation systems have been proposed in [4, 16–18, 24, 25]. To this end, the first prerequisite is a set of unitary matrices. To avoid this, Tarokh and Jafarkhani proposed a differential detection scheme for two transmit antennas in [19] and extended it to multiple transmit antennas in [11]. For the case when the receiver has CSI, super-orthogonal space-time trellis codes (SOSTTCs) have been introduced in [10]. Zhu and Jafarkhani presented in [26] two rather simple, fully connected trellis sections for binary phase-shift keying (BPSK) and quadriphase-shift keying (QPSK). The case of eight-phase shift keying (8PSK) is not treated in [26]. In contradistinction to [26], we consider all the three signal constellations, BPSK, QPSK and 8PSK and design differential super-orthogonal space-time trellis encoders based on nonfully connected trellises. Moreover, we use the differential scheme described in [19], while, as much as we understand, the authors of [26] prefer an older one, based on unitary matrices.

In [19], only differential BPSK modulation is described in detail for the case of two transmit antennas, while performance plots are also provided for QPSK and 8PSK. We made no attempt to consider 16PSK as well, since it has a rather small practical usefulness and the complexity grows unacceptably high, as the cardinality of the required matrix set is 256. Although we consider the differential scheme described in [19] as excellent, we propose a new decoding metric with exactly the same performance as that given in [19], but superior from the standpoint of the computing time.

The bit error rate (BER) performance of both coherent and noncoherent communication systems using SOSTTCs is evaluated by computer simulations based on a geometric two-ring channel model [12]. We take the opportunity of performing those simulations to study the impact of different channel parameters and transmission scenarios on the system performance. We compare the BER performance of the SOSTTCs using both the differential and the coherent encoding schemes. As known from the theory and practice of single antenna communication systems, the SOSTTCs using the differential encoding scheme are approximately 3 dB worse than those using the coherent scheme, and this is the price paid for having no need of CSI at the receiver.

The rest of the paper is organized as follows. In Section 2, we describe our channel model and develop the differential scheme for BPSK, QPSK and 8PSK. It will be clear that the matrix sets used for trellis-coding are quite different from those used for differential transmission. In Section 3, for fair comparison, we first design SOSTTCs to be included in coherent transmission systems. In Section 4, we design SOSTTCs that work together with differential detection and therefore have no need of CSI. Receiver issues are treated in Section 5, where the traditional decoding algorithm and the new decoding algorithm are presented. Simulation results and related comments are given in Section 6. Section 7 contains our conclusions.

2 Channel model and differential encoding

2.1 Channel model

We consider a point-to-point noncoherent wireless communication link with two transmit antennas and one or two receive antennas, operating in a Rayleigh flat-fading environment like in [19]. The signal constellation used for transmission is M-PSK, with $M = 2^b$ and $b = 1, 2$ and 3, i.e. BPSK, QPSK and 8PSK. The average energy of the symbols transmitted from each antenna is normalized to be 1/2, in order that the average power of the received signal at each received antenna is 1. Therefore, the 2D signal constellation is a set

$$S = \left\{ \frac{e^{2\pi kj/M}}{\sqrt{2}} \; | k = 0, 1, \ldots, M-1 \right\} \tag{1}$$

where $j^2 = -1$.

In our method, we use a 4D signal constellation that is the Cartesian product of a 2D signal constellation by itself. Denote the 2D symbol interval by T. A 4D symbol is transmitted in two consecutive time intervals of duration T and thus its duration equals $2T$. We number the 4D symbol intervals by n, $n = 0, 1, 2, \ldots$, and the first and the second half of the generic 4D symbol interval are denoted as $2n$ and $2n + 1$, respectively. Note that actually BPSK is not 2D, but 1D.

In this paper, we assume that the fading is constant over a time interval whose duration is at least equal to $4T$. Furthermore, let us denote the path gain from the transmit antenna q, $q = 1, 2$, to the receive antenna p, by $h_n^{(p,q)}$. The path gains are modelled as samples of independent complex Gaussian stochastic processes with variance 0.5 per real dimension.

2.2 Differential encoding

We assume that the data transmission is being made by frames, where by *frame* we understand a block of N 4D consecutive symbols, or equivalently of $2N$ 2D consecutive QPSK or 8PSK symbols, and of N 2D consecutive symbols, or equivalently of $2N$ 1D consecutive

BPSK symbols, that are maximum likelihood sequence decoded by the receiver using the Viterbi algorithm. For brevity of exposition, we consider 2D signal constellations, but the theory is the same for BPSK. We index the 4D symbols by $n, n = 0, 1, \ldots, N-1$. The nth 4D symbol comprises two consecutive 2D symbols denoted as s_{2n} and s_{2n+1} which are transmitted by the first antenna into two successive channel uses $2n$ and $2n+1$. The second antenna transmits the same information, but in a different order and form, i.e. $-a_n s^*_{2n+1}$ first and $a_n s^*_{2n}$ next, where the variable a_n can take the values $+1$ and -1 as it will be shown later. It is useful to consider these quantities as the entries of a 2×2 transmission matrix:

$$\mathbf{M}_n = \begin{pmatrix} s_{2n} & -a_n \cdot s^*_{2n+1} \\ s_{2n+1} & a_n \cdot s^*_{2n} \end{pmatrix}. \tag{2}$$

For a_n fixed as $+1$ or -1, we readily recognize in (2) the Alamouti matrix [3], which is also an orthogonal design, since the two columns, as well as the two rows, are orthogonal.

For coherent demodulation and a_n fixed, all the matrices that can be formed with symbols of a given signal constellation make up a signal set and a space-time trellis code can be designed by properly assigning a transmission matrix to each state transition of a topological trellis. Clearly, the data rate is determined by the cardinality of such a signal set. To increase the data rate by one bit per 4D symbol, the signal set is taken as the union of two families of matrices, one for $a_n = +1$ and the other one for $a_n = -1$. With this enlarged set of matrices, an SOSTTC can be built [10].

When no CSI is available at the receiver, only non-coherent demodulation can be used. As in [19], we consider the two orthogonal vectors $(s_{2n}, -a_n \cdot s^*_{2n+1})$ and $(s_{2n+1}, a_n \cdot s^*_{2n})$ having unit length. Then, any 2D vector $(s_{2n+2}, -a_n \cdot s^*_{2n+3})$ can be uniquely represented in the orthonormal basis given by these vectors. Assuming that the fading is constant at least over two consecutive 4D symbols, the information to be transmitted in the $(n+1)$th 4D symbol interval is differentially encoded as follows:

$$\begin{pmatrix} s_{2n+2} & -a_{n+1} \cdot s^*_{2n+3} \\ s_{2n+3} & a_{n+1} \cdot s^*_{2n+2} \end{pmatrix} = \begin{pmatrix} u_{2n+2} & u_{2n+3} \\ -a_n \cdot a_{n+1} \cdot u^*_{2n+3} & a_n \cdot a_{n+1} \cdot u^*_{2n+2} \end{pmatrix} \cdot \begin{pmatrix} s_{2n} & -a_n \cdot s^*_{2n+1} \\ s_{2n+1} & a_n \cdot s^*_{2n} \end{pmatrix} \tag{3}$$

where

$$u_{2n+2} = s^*_{2n} \cdot s_{2n+2} + a_n \cdot a_{n+1} \cdot s_{2n+1} \cdot s^*_{2n+3} \tag{4}$$

and

$$u_{2n+3} = s_{2n+2} \cdot s^*_{2n+1} - a_n \cdot a_{n+1} \cdot s_{2n} \cdot s^*_{2n+3}. \tag{5}$$

From (3), we also have that

$$s_{2n+2} = u_{2n+2} \cdot s_{2n} + u_{2n+3} \cdot s_{2n+1} \tag{6}$$

$$s_{2n+3} = a_n \cdot a_{n+1} \left(u^*_{2n+2} \cdot s_{2n+1} - u^*_{2n+3} \cdot s_{2n} \right). \tag{7}$$

We call *transmission matrix* a matrix whose entries, denoted by the letter s, are transmitted from the two transmit antennas, and *encoding matrix*, a matrix whose entries are denoted by the letter u. The encoding matrices are used to label the state transitions of the trellis diagram. Define the encoding matrix as

$$\mathbf{ME}_{n+1} = \begin{pmatrix} u_{2n+2} & -a_n \cdot a_{n+1} \cdot u^*_{2n+3} \\ u_{2n+3} & a_n \cdot a_{n+1} \cdot u^*_{2n+2} \end{pmatrix}. \tag{8}$$

Then, the encoding equation (3) can be written as

$$\mathbf{M}_{n+1} = \mathbf{ME}^T_{n+1} \cdot \mathbf{M}_n. \tag{9}$$

It is easy to see that, if the entries of the transmission matrices are signal points from an M-PSK constellation, unfortunately, the entries of the encoding matrices are *not*.

The general structure of our transmission system is depicted in Fig. 1.

2.3 Signal constellations for trellis coding

In trellis-coded modulation, the signal constellation, which is double-sized compared with the one used by the uncoded system, is partitioned into two equal-sized subsets called families and denoted as F_0 and F_1 [21, 22]. In our paper, the family F_0 comprises all encoding matrices with $a_n a_{n+1} = 1$, while the family F_1 comprises all encoding matrices with $a_n a_{n+1} = -1$. For each matrix belonging to F_0, there is a matrix in F_1 having the same first column, but a different second one. The two matrices are selected by blocks of bits at the output of a systematic feedback convolutional encoder differing only in the least significant bit, i.e. $c0_{n+1} = 0$ for F_0 and $c0_{n+1} = 1$ for F_1. The differential encoding according to (4) and (5) depends on both (s_{2n}, s_{2n+1}) and (s_{2n+2}, s_{2n+3}). To select the corresponding 4D symbol (u_{2n+2}, u_{2n+3}), only $2b$ input bits are available, while twice as much bits would have been necessary to select an 8D symbol $(s_{2n}, s_{2n+1}, s_{2n+2}, s_{2n+3})$. The $2b$ input bits can select one out of 2^{2b} vectors (u_{2n+2}, u_{2n+3}) that transform a given 4D signal point (s_{2n}, s_{2n+1}) into the next one (s_{2n+2}, s_{2n+3}). To establish a bijection, a possibility is to fix a point (for instance, $s_{2n} = s_{2n+1} = 1/\sqrt{2}$ as in [19]) and use it for all other 4D signal points (s_{2n}, s_{2n+1}).

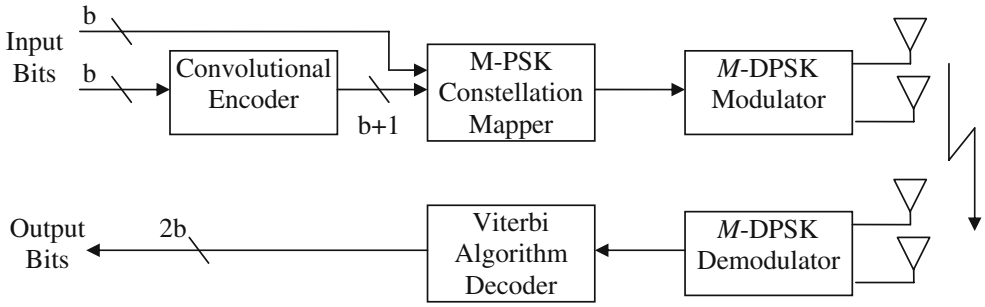

Fig. 1 Transceiver structure of super-orthogonal space-time trellis encoded M-DPSK for fading channels

Consider first BPSK, which uses a 1D signal constellation and is equivalent to binary amplitude shift keying (BASK). In the $(n+1)$th 2D symbol interval, two consecutive source bits, denoted as $b1_{2n+2}$ and $b1_{2n+3}$, are presented at the input of a systematic convolutional encoder whose output comprises three bits: $c0_{n+1}, c1_{n+1} = b1_{2n+2}$ and $c2_{n+1} = b1_{2n+3}$. There must be a bijective mapping of the set of dibits $\{c1_{n+1},\ c2_{n+1}\}$ onto the set of encoding symbols $\{u_{2n+2},\ u_{2n+3}\}$. Following [19], we fix $s_{2n} = s_{2n+1} = 1/\sqrt{2}$ in (3) and (4). For this particular case, we have

$$u_{2n+2} = \left(s_{2n+2} + a_n \cdot a_{n+1} \cdot s^*_{2n+3}\right)/\sqrt{2} \tag{10}$$

$$u_{2n+3} = \left(s_{2n+2} - a_n \cdot a_{n+1} \cdot s^*_{2n+3}\right)/\sqrt{2}\,. \tag{11}$$

The signal points, computed with (4) and (5), are listed in Table 1. Note that, in contradistinction to the 1D signal constellation constituent of the 2D signal constellation used for transmission, which has only two points $-1/\sqrt{2}$ and $+1/\sqrt{2}$, that one used for trellis encoding comprises three points: $+1$, -1 and 0.

Next, we consider QPSK. In the $(n+1)$th 4D symbol interval, four consecutive source bits, denoted as $b1_{2n+2}$, $b2_{2n+2}$, $b1_{2n+3}$ and $b2_{2n+3}$, are fed to a systematic convolutional encoder whose output comprises five bits: $c0_{n+1}, c1_{n+1} = b1_{2n+2}, c2_{n+1} = b2_{2n+2}, c3_{n+1} = b1_{2n+3}$ and $c4_{n+1} = b2_{2n+3}$. When fixing $s_{2n} = s_{2n+1} = 1/\sqrt{2}$ as for BPSK, the result of the computation using (8) and (9) is given in Table 2. Note that, with this mapping, (6) and (7) will result into QPSK symbols only if the product $s_{2n} \cdot s_{2n+1}$ is a real number. However, when this product is an imaginary number, it is easy to verify that some of the symbols computed with (6) and (7) do not belong to QPSK.

Finally, we consider 8PSK. In the $(n+1)$th 4D symbol interval, six consecutive source bits, denoted as $b1_{2n+2}$, $b2_{2n+2}$, $b3_{2n+2}$, $b1_{2n+3}$, $b2_{2n+3}$ and $b3_{2n+3}$, are fed to a systematic convolutional encoder whose output comprises seven bits: $c0_{n+1}, c1_{n+1} = b1_{2n+2}, c2_{n+1} = b2_{2n+2}, c3_{n+1} = b3_{2n+2}, c4_{n+1} = b1_{2n+3}, c5_{n+1} = b2_{2n+3}$ and $c6_{n+1} = b3_{2n+3}$. The mapping of the selection bits onto the encoding symbols is given in Table 3. Note that, for convenience, the shorthand notation $a = a_n \cdot a_{n+1}$ was used.

We make here the same comment as in the case of QPSK: when the product $s_{2n} \cdot s_{2n+1}$ is complex-valued, using (6) and (7) results into some symbols that do not belong to 8PSK. Fortunately, this has no detrimental effect on the receiver, since the carrier phase is not recovered.

Table 1 Mapping of selection bits into 2D BPSK signal points

Subset	$c2_{n+1}$	$c1_{n+1}$	u_{2n+2}	u_{2n+3}
SD_0	0	0	1	0
	1		−1	0
SD_1	0	1	0	−1
	1		0	1

Table 2 Mapping of selection bits into 4D QPSK signal points

Subset	$c4_{n+1}$	$c3_{n+1}$	$c2_{n+1}$	$c1_{n+1}$	u_{2n+2}	u_{2n+3}
SD_0	0	0	0	0	1	0
	0	1			0	j
	1	0			0	$-j$
	1	1			−1	0
SD_1	0	0	0	1	$(1-j)/2$	$(1+j)/2$
	0	1			$-(1-j)/2$	$(1+j)/2$
	1	0			$(1-j)/2$	$-(1+j)/2$
	1	1			$-(1-j)/2$	$-(1+j)/2$
SD_2	0	0	1	0	$(1+j)/2$	$(1-j)/2$
	0	1			$(1+j)/2$	$-(1-j)/2$
	1	0			$-(1+j)/2$	$(1-j)/2$
	1	1			$-(1+j)/2$	$-(1-j)/2$
SD_3	0	0	1	1	0	1
	0	1			j	0
	1	0			$-j$	0
	1	1			0	−1

Table 3 Mapping of selection bits into 4D 8PSK signal points

Subset	$c6_{n+1}$	$c5_{n+1}$	$c4_{n+1}$	$c3_{n+1}$	$c2_{n+1}$	$c1_{n+1}$	u_{2n+2}	u_{2n+3}
SD_0	0	0	0	0	0	0	1	0
	0	0	1				$\sqrt{2}/2$	$j\sqrt{2}/2$
	0	1	0				$-\sqrt{2}/2$	$j\sqrt{2}/2$
	0	1	1				$j(1-a)/2$	$j(1+a)/2$
	1	0	0				$\sqrt{2}/2$	$-j\sqrt{2}/2$
	1	0	1				0	$-j$
	1	1	0				–1	0
	1	1	1				$-\sqrt{2}/2$	$-j\sqrt{2}/2$
SD_1	0	0	0	0	0	1	$(2+\sqrt{2}-j\sqrt{2})/4$	$(2-\sqrt{2}+j\sqrt{2})/4$
	0	0	1				$[\sqrt{2}-j(2-\sqrt{2})]/4$	$[\sqrt{2}+j(2+\sqrt{2})]/4$
	0	1	0				$-[2+\sqrt{2}-j\sqrt{2}]/4$	$[2-\sqrt{2}+j\sqrt{2}]/4$
	0	1	1				$-[\sqrt{2}-j(2-\sqrt{2})]/4$	$[\sqrt{2}+j(2+\sqrt{2})]/4$
	1	0	0				$(2+\sqrt{2}-j\sqrt{2})/4$	$-(2-\sqrt{2}+j\sqrt{2})/4$
	1	0	1				$[\sqrt{2}-j(2-\sqrt{2})]/4$	$-[\sqrt{2}+j(2+\sqrt{2})]/4$
	1	1	0				$-[2+\sqrt{2}-j\sqrt{2}]/4$	$-[2-\sqrt{2}+j\sqrt{2}]/4$
	1	1	1				$-[\sqrt{2}-j(2-\sqrt{2})]/4$	$-[\sqrt{2}+j(2+\sqrt{2})]/4$
SD_2	0	0	0	0	1	0	$(2-\sqrt{2}-j\sqrt{2})/4$	$(2+\sqrt{2}+j\sqrt{2})/4$
	0	0	1				$(\sqrt{2}-2+j\sqrt{2})/4$	$(2+\sqrt{2}+j\sqrt{2})/4$
	0	1	0				$-[\sqrt{2}-j(2+\sqrt{2})]/4$	$-[\sqrt{2}+j(2-\sqrt{2})]/4$
	0	1	1				$-[\sqrt{2}-j(2+\sqrt{2})]/4$	$[\sqrt{2}+j(2-\sqrt{2})]/4$
	1	0	0				$[\sqrt{2}-j(2+\sqrt{2})]/4$	$[\sqrt{2}+j(2-\sqrt{2})]/4$
	1	0	1				$[\sqrt{2}-j(2+\sqrt{2})]/4$	$-[\sqrt{2}-j(2-\sqrt{2})]/4$
	1	1	0				$-[2-\sqrt{2}-j\sqrt{2}]/4$	$-[2+\sqrt{2}+j\sqrt{2}]/4$
	1	1	1				$(2-\sqrt{2}+j\sqrt{2})/4$	$-(2+\sqrt{2}-j\sqrt{2})/4$
SD_3	0	0	0	0	1	1	$(1-j)/2$	$(1+j)/2$
	0	0	1				0	$\sqrt{2}(1+j)/2$
	0	1	0				$-\sqrt{2}(1-j)/2$	0
	0	1	1				$-(1-j)/2$	$(1+j)/2$
	1	0	0				$\sqrt{2}(1-j)/2$	0
	1	0	1				$(1-j)/2$	$-(1+j)/2$
	1	1	0				$-(1-j)/2$	$-(1+j)/2$
	1	1	1				0	$-\sqrt{2}(1+j)/2$
SD_4	0	0	0	1	0	0	$(2+\sqrt{2}+j\sqrt{2})/4$	$(2-\sqrt{2}-j\sqrt{2})/4$
	0	0	1				$(2+\sqrt{2}+j\sqrt{2})/4$	$(\sqrt{2}-2+j\sqrt{2})/4$
	0	1	0				$-[\sqrt{2}+j(2-\sqrt{2})]/4$	$-[\sqrt{2}-j(2+\sqrt{2})]/4$
	0	1	1				$[\sqrt{2}+j(2-\sqrt{2})]/4$	$[-\sqrt{2}+j(2+\sqrt{2})]/4$
	1	0	0				$[\sqrt{2}+j(2-\sqrt{2})]/4$	$[\sqrt{2}-j(2+\sqrt{2})]/4$
	1	0	1				$-[\sqrt{2}+j(2-\sqrt{2})]/4$	$[\sqrt{2}-j(2+\sqrt{2})]/4$
	1	1	0				$-(2+\sqrt{2}+j\sqrt{2})/4$	$-(2-\sqrt{2}-j\sqrt{2})/4$
	1	1	1				$-(2+\sqrt{2}+j\sqrt{2})/4$	$(2-\sqrt{2}-j\sqrt{2})/4$
SD_5	0	0	0	1	0	1	$(1+j)/2$	$(1-j)/2$
	0	0	1				$\sqrt{2}(1+j)/2$	0
	0	1	0				0	$-\sqrt{2}(1-j)/2$
	0	1	1				$(1+j)/2$	$-(1-j)/2$
	1	0	0				0	$\sqrt{2}(1-j)/2$
	1	0	1				$-(1+j)/2$	$(1-j)/2$
	1	1	0				$-(1+j)/2$	$-(1-j)/2$
	1	1	1				$-\sqrt{2}(1+j)/2$	0
SD_6	0	0	0	1	1	0	0	1
	0	0	1				$j\sqrt{2}/2$	$\sqrt{2}/2$
	0	1	0				$j\sqrt{2}/2$	$-\sqrt{2}/2$
	0	1	1				j	0
	1	0	0				$-j\sqrt{2}/2$	$\sqrt{2}/2$
	1	0	1				$-j$	0
	1	1	0				0	–1
	1	1	1				$-\sqrt{2}/2$	$-\sqrt{2}/2$

Table 3 (continued)

Subset	$c6_{n+1}$	$c5_{n+1}$	$c4_{n+1}$	$c3_{n+1}$	$c2_{n+1}$	$c1_{n+1}$	u_{2n+2}	u_{2n+3}
SD_7	0	0	0	1	1	1	$[2-\sqrt{2}+j\sqrt{2}]/4$	$[2+\sqrt{2}-j\sqrt{2}]/4$
	0	0	1				$[\sqrt{2}+j(2+\sqrt{2})]/4$	$[\sqrt{2}-j(2-\sqrt{2})]/4$
	0	1	0				$(2-\sqrt{2}+j\sqrt{2})/4$	$-(2+\sqrt{2}-j\sqrt{2})/4$
	0	1	1				$[\sqrt{2}+j(2+\sqrt{2})]/4$	$-[\sqrt{2}-j(2-\sqrt{2})]/4$
	1	0	0				$-[2-\sqrt{2}+j\sqrt{2}]/4$	$[2+\sqrt{2}-j\sqrt{2}]/4$
	1	0	1				$-[\sqrt{2}+j(2+\sqrt{2})]/4$	$[\sqrt{2}-j(2-\sqrt{2})]/4$
	1	1	0				$-(2-\sqrt{2}+j\sqrt{2})/4$	$-(2+\sqrt{2}-j\sqrt{2})/4$
	1	1	1				$-[\sqrt{2}+j(2+\sqrt{2})]/4$	$-[\sqrt{2}-j(2-\sqrt{2})]/4$

3 Super-orthogonal space-time trellis codes for coherent detection

In this section, we present SOSTTCs for coherent detection that are used as references for the new codes, designed for noncoherent communications systems. We do this in a somewhat expedite manner, since such codes are rather well known [10, 15].

It is useful to see a signal point s of coordinates (x, y) as a complex number $x + jy$. To measure the difference between two transmission matrices $\mathbf{M}_n^{(1)}$ and $\mathbf{M}_n^{(2)}$ as defined by (2), we use the *coding gain distance* (CGD), defined in [10] as follows. Define $\mathbf{B}_n = \mathbf{M}_n^{(1)} - \mathbf{M}_n^{(2)}$ and form the matrix $\mathbf{A}_n = \mathbf{B}_n \cdot \mathbf{B}_n^H$, where $\mathbf{B}_n^H$ is the Hermitian (complex conjugate and transpose) of $\mathbf{B}_n$. Then, $d^2 = \det(\mathbf{A}_n)$. Note that this is actually the squared Euclidian distance between two 4D signal points $(x_{2n}^{(1)},\ y_{2n}^{(1)},\ x_{2n+1}^{(1)},\ y_{2n+1}^{(1)})$ and $(x_{2n}^{(2)},\ y_{2n}^{(2)},\ x_{2n+1}^{(2)},\ y_{2n+1}^{(2)})$:

$$d^2 = \sum_{i=0}^{1} \left[\left(x_{2n+i}^{(1)} - x_{2n+i}^{(2)} \right)^2 + \left(y_{2n+i}^{(1)} - y_{2n+i}^{(2)} \right)^2 \right] . \quad (12)$$

Obviously, the larger the difference of the respective coordinates, the larger is the CGD. Following [10], we define the parameter $\omega = 2\pi/M$. Assuming a circle of radius $1/\sqrt{2}$ centred in the origin, we then express the coordinates x_{2n+i} and y_{2n+i}, $i = 0, 1$, as

$$x_{2n+i} = \frac{1}{\sqrt{2}} \cos k_{2n+i}\, \omega \quad (13)$$

and

$$y_{2n+i} = \frac{1}{\sqrt{2}} \sin k_{2n+i}\, \omega \, . \quad (14)$$

Inserting (13) and (14) into (12), we easily obtain:

$$d^2 = \sum_{i=0}^{1} \left[1 - \cos \left(k_{2n+i}^{(1)} - k_{2n+i}^{(2)} \right) \omega \right]^2 . \quad (15)$$

3.1 SOSTTCs for BPSK

The BPSK signal constellation is illustrated in Fig. 2. The two 1D signal points are labelled as 0 and 1. In this very particular case, the natural and the Gray mapping coincide, and BPSK is equivalent to BASK: a bit 0 is transmitted as the amplitude $1/\sqrt{2}$, while a bit 1 is transmitted as the amplitude $-1/\sqrt{2}$. Grouping the 1D points into 2D points, we obtain four 2D points: (0, 0), (0, 1), (1, 0) and (1, 1). We partition this set into two subsets S_0 and S_1 such that the intrasubset Hamming distance is maximized to 2:

$$S_0 = \{(0,0)\,,\ (1,1)\} \quad (16)$$

$$S_1 = \{(0,1)\,,\ (1,0)\}\ . \quad (17)$$

In two consecutive signalling intervals $2n$ and $2n+1$, two bits are gathered at the input of the transmitter, denoted by $b1_{2n}$ and $b1_{2n+1}$. A 2D signal point is the concatenation of two 1D points that are transmitted by BPSK in two consecutive signalling periods. The bit $b1_{2n}$ is encoded by a rate-1/2 systematic convolutional encoder, while the bit $b1_{2n+1}$ remains uncoded and, for convenience, is denoted as $c2_n$ at the input of the BPSK mapper. The rate-1/2 convolutional encoder outputs two bits, denoted by $c0_n$ and $c1_n$ such that $c1_n = b1_{2n}$.

Consider the orthogonal matrices defined by (2). They form two families F_0 (with $a_n = +1$) and F_1 (with $a_n = -1$), selected by $c0_n = 0$ and $c0_n = 1$, respectively. Moreover, each family is further partitioned in subsets of matrices and denoted as $\mathbf{SM}_p$, such that the index of a matrix subset $\mathbf{SM}_p$ is given by

$$p = 2c1_n + c0_n\, . \quad (18)$$

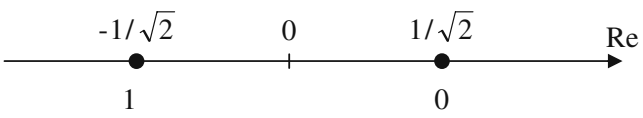

Fig. 2 BPSK signal constellation

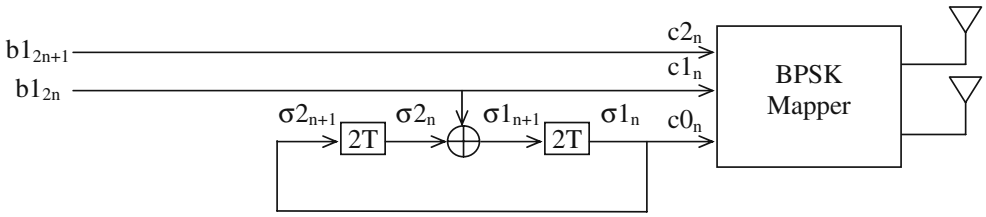

Fig. 3 Super-orthogonal space-time trellis encoder for BPSK signal constellation

The first antenna transmits consecutively the symbols s_{2n} and s_{2n+1} from the BPSK signal constellation. However, for $c0_n = 0$ and $c0_n = 1$, the second antenna will transmit data symbols according to the matrix pattern with $a_n = +1$ and $a_n = -1$, respectively.

To select a point from a 1D BPSK constellation, constituent of a 2D constellation, a bit is required, denoted by $z1_i$, where $i \in \{2n,\ 2n+1\}$. The convolutionally encoded bit $c1_n$ (actually, the input bit $b1_{2n}$) selects a 2D subset that is the set of all 2D points for which the following relation holds true:

$$z1_{2n+1} = c1_n \oplus z1_{2n}\,. \tag{19}$$

Then, the index m of the subset S_m, $m = 0, 1$, is given by $m = z1_{2n} \oplus z1_{2n+1}$.

The uncoded input bit $b1_{2n+1}$ determines the 2D signal point within the already selected 2D subset to be transmitted by the first antenna in two consecutive signalling intervals $2n$ and $2n+1$ such that $z1_{2n} = b1_{2n+1}$.

In the context of space-time trellis coding, the TCM rules given by Ungerboeck [21–23] sound as follows:

1. The state transitions originating in even-numbered states are assigned transmission matrices belonging to the family F_0, and the state transitions originating in odd-numbered states are assigned transmission matrices belonging to the family F_1.
2. The state transitions reaching the same next state are assigned transmission matrices from the same family, be it F_0 or F_1.

Define two binary state variables $\sigma 1_n$ and $\sigma 2_n$ such that the decimal value of the current state is written as $\sigma_n = 2\sigma 2_n + \sigma 1_n$. Using Ungerboeck's rules to assign orthogonal matrices to the state transitions of a four-state topological trellis [21], we derive the block diagram of the SOSTTC encoder given in Fig. 3. SOSTTCs with a larger number of states can be built in a similar way.

3.2 SOSTTCs for QPSK

The QPSK signal constellation, with natural and, in parentheses, Gray mapping, is illustrated in Fig. 4. For coherent demodulation, the natural mapping will do. The four 2D signal points are labelled as 0, 1, 2 and 3. By grouping them into 4D points, we obtain 16 points from (0, 0) to (3, 3). With those points, we then form the following 4D subsets:

$$S_0 = \{(0,0), (1,1), (2,2), (3,3)\} \tag{20}$$

$$S_1 = \{(0,1), (1,2), (2,3), (3,0)\} \tag{21}$$

$$S_2 = \{(0,2), (1,3), (2,0), (3,1)\} \tag{22}$$

$$S_3 = \{(0,3), (1,0), (2,1), (3,2)\}\,. \tag{23}$$

To select one out of four subsets S_m, $m = 0, \ldots, 3$, two bits are required, say, $c1_n$ and $c2_n$, such that the index m can be written as $m = 2c2_n + c1_n$.

In two consecutive signalling intervals $2n$ and $2n+1$, four bits are gathered at the input of the transmitter, denoted by $b1_{2n}$, $b2_{2n}$, $b1_{2n+1}$, $b2_{2n+1}$. The first two bits, $b1_{2n}$ and $b2_{2n}$, are encoded by a rate-2/3 systematic convolutional encoder, while the next two bits, $b1_{2n+1}$ and $b2_{2n+1}$, remain uncoded. The rate-2/3 convolutional encoder outputs three bits, denoted by $c0_n$, $c1_n$ and $c2_n$, such that $c1_n = b1_{2n}$ and $c2_n = b2_{2n}$.

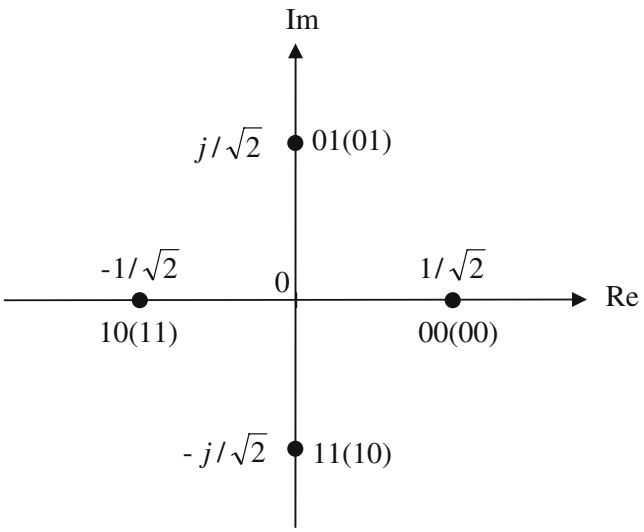

Fig. 4 QPSK signal constellation with natural mapping and, in parentheses, Gray mapping

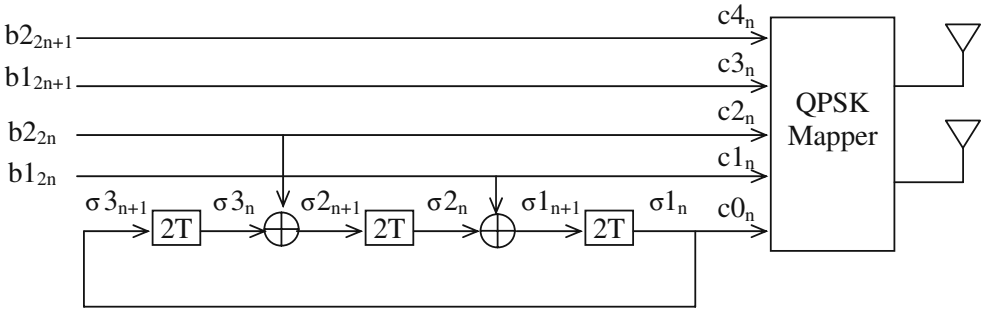

Fig. 5 Super-orthogonal space-time trellis encoder for QPSK signal constellation

For QPSK, the index of a matrix subset SM_p is given by

$$p = 4c2_n + 2c1_n + c0_n \,. \tag{24}$$

To select a point from a 2D QPSK constellation, constituent of a 4D constellation, two bits are required, denoted by $z1_i$, $z2_i$, where $i \in \{2n,\ 2n+1\}$. The two bits $(z2_i\ z1_i)$ select a 2D signal point as shown in Fig. 4.

The two convolutionally encoded bits $c1_n$ and $c2_n$ (actually, the input bits $b1_{2n}$ and $b2_{2n}$) select a 4D subset that is the set of all 4D signal points for which (19) and (25) below hold true:

$$z2_{2n+1} = c2_n \oplus z2_{2n} \oplus (c1_n \cdot z1_{2n}) \,. \tag{25}$$

The two uncoded input bits, $b1_{2n+1}$ and $b2_{2n+1}$, determine the 4D signal point within the already selected 4D subset to be transmitted by the first antenna in two consecutive signalling intervals $2n$ and $2n+1$ such that $z1_{2n} = b1_{2n+1}$ and $z2_{2n} = b2_{2n+1}$.

Define three binary state variables $\sigma 1_n$, $\sigma 2_n$, and $\sigma 3_n$ such that the decimal value of the current state is written as $\sigma_n = 4\sigma 3_n + 2\sigma 2_n + \sigma 1_n$. Using the same TCM rules as before, we derive the logic diagram given in Fig. 5.

3.3 SOSTTCs for 8PSK

The 8PSK signal constellation, with natural and, in parentheses, Gray mapping, is illustrated in Fig. 6. The eight 2D points are labelled from 0 to 7. Grouping them into 4D points, we get 64 4D points from (0, 0) to (7, 7). With those points, we form the following 4D subsets:

$$S_0 = \{(0,0),\ (1,1),\ (2,2),\ (3,3),\ (4,4),\ (5,5),\ (6,6),\ (7,7)\} \tag{26}$$

$$S_1 = \{(0,1),\ (1,2),\ (2,3),\ (3,4),\ (4,5),\ (5,6),\ (6,7),\ (7,0)\} \tag{27}$$

$$S_2 = \{(0,2),\ (1,3),\ (2,4),\ (3,5),\ (4,6),\ (5,7),\ (6,0),\ (7,1)\} \tag{28}$$

$$S_3 = \{(0,3),\ (1,4),\ (2,5),\ (3,6),\ (4,7),\ (5,0),\ (6,1),\ (7,2)\} \tag{29}$$

$$S_4 = \{(0,4),\ (1,5),\ (2,6),\ (3,7),\ (4,0),\ (5,1),\ (6,2),\ (7,3)\} \tag{30}$$

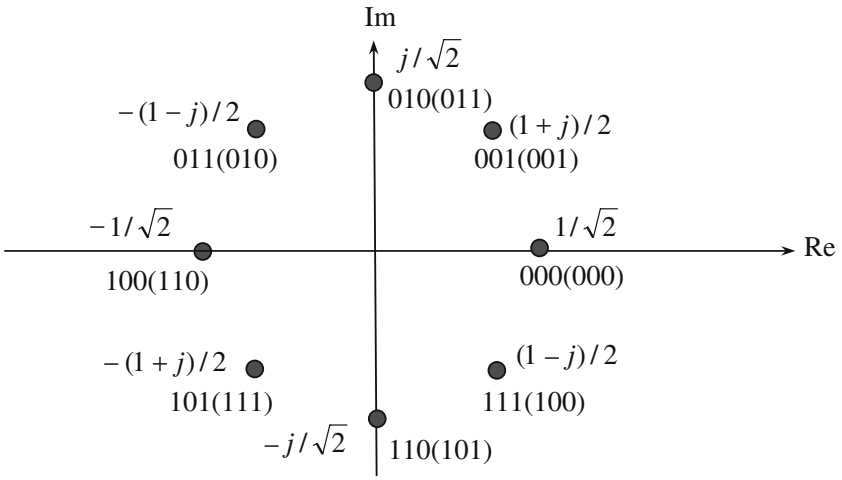

Fig. 6 8PSK signal constellation with natural mapping and, in parenthesis, Gray mapping

$$S_5 = \{(0,5), (1,6), (2,7), (3,0), (4,1), (5,2), (6,3), (7,4)\} \tag{31}$$

$$S_6 = \{(0,6), (1,7), (2,0), (3,1), (4,2), (5,3), (6,4), (7,5)\} \tag{32}$$

$$S_7 = \{(0,7), (1,0), (2,1), (3,2), (4,3), (5,4), (6,5), (7,6)\}\,. \tag{33}$$

To select one out of eight subsets S_m, $m = 0, \cdots, 7$, three bits are required, say, $c1_n$, $c2_n$ and $c3_n$ such that the index m can be written as $m = 4c3_n + 2c2_n + c1_n$.

In two consecutive signalling intervals $2n$ and $2n+1$, six bits are gathered at the input of the transmitter, denoted by $b1_{2n}$, $b2_{2n}$, $b3_{2n}$, $b1_{2n+1}$, $b2_{2n+1}$, $b3_{2n+1}$. The first three bits are encoded by a rate-3/4 systematic convolutional encoder, while the other three bits remain uncoded. The rate-3/4 convolutional encoder outputs four bits, denoted by $c0_n$, $c1_n$, $c2_n$ and $c3_n$, such that $c1_n = b1_{2n}$, $c2_n = b2_{2n}$ and $c3_n = b3_{2n}$.

For 8PSK, the index p of a matrix subset SM_p is given by

$$p = 8c3_n + 4c2_n + 2c1_n + c0_n\,. \tag{34}$$

To select a point from a 2D 8PSK constellation, constituent of a 4D constellation, three bits are required, denoted by $z1_i$, $z2_i$, and $z3_i$, where $i \in \{2n, 2n+1\}$. These three bits select a 2D signal point according to the natural mapping as shown in Fig. 6.

The three convolutionally encoded bits $c1_n$, $c2_n$ and $c3_n$ (actually, the input bits $b1_{2n}$, $b2_{2n}$ and $b3_{2n}$) select a 4D subset that is the set of all 4D signal points for which (19), (25) and (35) below hold true:

$$z3_{2n+1} = c3_n \oplus z3_{2n} \oplus [c2_n \cdot z2_{2n} + (c2_n \oplus z2_{2n}) \cdot (c1_n \cdot z1_{2n})]\,. \tag{35}$$

The three uncoded input bits $b1_{2n+1}$, $b2_{2n+1}$, and $b3_{2n+1}$, determine the 4D signal point within the already selected 4D subset to be transmitted by the first antenna in two consecutive signalling intervals $2n$ and $2n+1$ such that $z1_{2n} = b1_{2n+1}$, $z2_{2n} = b2_{2n+1}$ and $z3_{2n} = b3_{2n+1}$.

Define four binary state variables $\sigma 1_n$, $\sigma 2_n$, $\sigma 3_n$ and $\sigma 4_n$ such that the decimal value of the current state is written as $\sigma_n = 8\sigma 4_n + 4\sigma 3_n + 2\sigma_n + \sigma 1_n$. The resulting logic diagram is given in Fig. 7. The easy way of selection, as reflected in (19), (25) and (35), is explained by the clever partition of the 4D signal constellation into $M = 2^b$ subsets: the generic subset S_m contains the points $\{(0, m), (1, m+1), \ldots, (M-1, M+m-1 \mod M)\}$. We claim that any other partition would require a rather complex look-up table, with no special advantage. This is also well explained in [15].

4 Super-orthogonal space-time trellis codes for noncoherent detection

In this section, we present the main contribution of our paper, i.e. SOSTTCs for communication systems having no knowledge of CSI. To this end, the differential encoding scheme developed in Section 2 is added to the SOSTTCs designed for coherent demodulation as explained in the following. To reflect the differential encoding, we now consider $n+1$ as the time index of the 4D (2D in case of BPSK) current symbol and, accordingly, $2n+2$ and $2n+3$ as the time indices of the two consecutive 2D (1D in case of BPSK) signal symbols. The signal constellation is the collection of all two-tuples (u_{2n+2}, u_{2n+3}) as given in Tables 1–3. Using the TCM rules, those symbols are assigned to state transitions of a topological trellis. Having in view that the mappings given in the said tables are bijective, this is equivalent to assigning vectors of selection bits to the state transitions.

For BPSK, the mapping of selection bits into 2D signal points (u_{2n+2}, u_{2n+3}) is shown in Table 1, where we also group the four 2D signal points into two subsets SD_0 and SD_1. Two bits are required to select a 2D point, $c1_{n+1}$ to select the subset and $c2_{n+1}$ to select the point within the selected subset. The input bit $b1_{2n+2}$ is encoded by a rate-1/2 systematic convolutional encoder just as in the coherent case and is denoted by $c1_{n+1}$ at the output.

The mapping of selection bits into 4D QPSK signal points (u_{2n+2}, u_{2n+3}) is given in Table 2, where the 16 4D signal points are grouped into four subsets SD_0, SD_1, SD_2 and SD_3. Table 3 shows how to map selection bits into 4D 8PSK signal points and subsets. The block diagrams of the SOSTTC encoder for BPSK signal constellation, QPSK constellation and 8PSK signal constellation look similar to those given in Figs. 3, 5, and 7, respectively, but the mapping includes the differential encoding as well.

The main contradistinction to the coherent case is that the output of the convolutional encoder does not select the 4D signal point to be transmitted by the first antenna in two consecutive signalling intervals as well as the pattern of the Alamouti transmission matrix, but the complex-valued two-tuple (u_{2n+2}, u_{2n+3}) as well as the pattern of the differential encoding matrix, as given in (3). The 4D (2D in case of BPSK) signal constellations used for differential encoding are 2^{2b}-

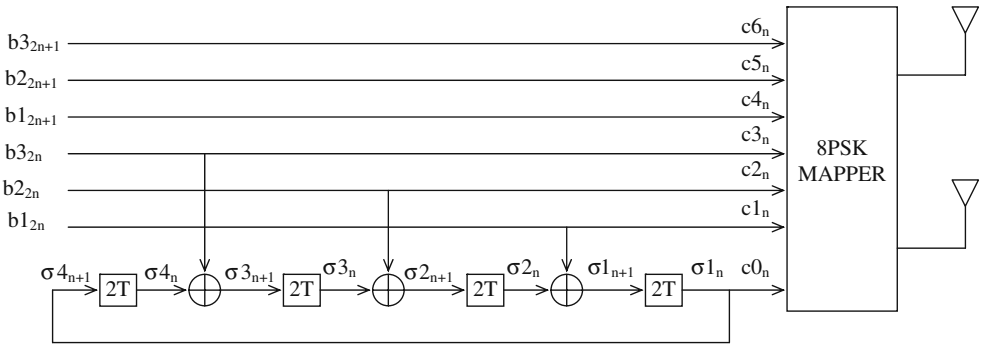

Fig. 7 Super-orthogonal space-time trellis encoder for 8-PSK signal constellation

point sets, where a 4D (2D in case of BPSK) signal point is a two-tuple $(u_{2n+2},\ u_{2n+3})$ of complex-valued symbols. It seems not very useful to consider such a 4D signal constellation as the Cartesian product of a 2D signal constellation by itself. Therefore, the selection procedure is somewhat different from that used for coherent detection. Another important contradistinction to the coherent case is that the convolutionally encoded bit $c0_{n+1}$ selects the encoding matrix family as follows: when $c0_{n+1} = 0$, then $a_n \cdot a_{n+1} = +1$, and when $c0_{n+1} = 1$, then $a_n \cdot a_{n+1} = -1$. Note that, for each originating state at time $n+1$, the value of a_n is known because of the second TCM rule, stating that all state transitions arriving in the same next state are assigned matrices from the same family, and thus, having the same a_n.

5 Receiver issues

5.1 Channel model for simulations

For the convenience of the reader, we insert here a short description of the MIMO channel simulator developed from a two-ring reference channel model that was employed to evaluate the performance of the SOSTTCs. In this model, it is assumed that local scatterers are located on two individual rings around the transmitter and the receiver. Homogeneous plane waves emitted from the transmitter are bounced only by the scatterers around the receiver. Assuming that the transmitter and the receiver are equipped with M_T transmit antennas and M_R receive antennas, the complex channel gains of the channel simulator can be expressed as [12]

$$h_{kl}(t) = \frac{1}{\sqrt{2M_s}} \sum_{m=1}^{M_s} a_{l,m}\, b_{k,m}\, e^{j(2\pi f_{1,m} t + \theta_{1,m})} + \frac{1}{\sqrt{2N_s}} \sum_{n=1}^{N_s} c_{l,n}\, d_{k,n}\, e^{j(2\pi f_{2,n} t + \theta_{2,n})} \tag{36}$$

for $l = 1, 2, \ldots, M_T$ and $k = 1, 2, \ldots, M_R$. In (36), M_s and N_s denote the number of local scatterers placed around the transmitter and the receiver, respectively. The quantities $f_{1,m}$ and $f_{2,n}$ represent the Doppler frequencies, as defined in [12]. The phases $\theta_{1,m}$ and $\theta_{2,n}$ are considered as outcomes from a random generator uniformly distributed over $(0, 2\pi]$. Furthermore, we have

$$a_{l,m} = e^{j\pi (M_T - 2l + 1)\frac{\delta_T}{\lambda} \cos\left(\phi_{T_1}^{(m)} - \beta_T\right)} \tag{37a}$$

$$b_{k,m} = e^{j\pi (M_R - 2k + 1)\frac{\delta_R}{\lambda} \left[\phi_R^{\max} \sin \phi_{T_1}^{(m)} \sin \beta_R - \cos \beta_R\right]} \tag{37b}$$

$$c_{l,m} = e^{j\pi (M_T - 2l + 1)\frac{\delta_T}{\lambda} \left[\phi_T^{\max} \sin \phi_{R_2}^{(n)} \sin \beta_T + \cos \beta_T\right]} \tag{37c}$$

$$d_{k,m} = e^{j\pi (M_R - 2k + 1)\frac{\delta_R}{\lambda} \cos\left(\phi_{R_2}^{(n)} - \beta_R\right)}. \tag{37d}$$

In the equations presented above, the antenna spacings at the transmitter and the receiver are denoted by δ_T and δ_R, respectively, and the orientations of the antenna arrays are described by β_T and β_R. The carrier's wavelength is denoted by λ. The angle $\phi_{T_1}^{(m)}$ represents the angle of departure (AOD), while the angle of arrival is described by $\phi_{R_2}^{(n)}$. The angle $\phi_R^{\max}$ describes one half of the maximum angle of arrival (AOA) observed at the receiver, while $\phi_T^{\max}$ is one half of the maximum AOD observed at the transmitter.

In this paper, we employ the von Mises distribution [1] to characterize the distribution of the AODs and the AOAs. For the channel simulator, both the AODs and the AOAs are determined by the modified method of equal area (MMEA) [6].

5.2 Decoding of SOSTTCs for known CSI at the receiver

Consider first the case of a single receive antenna. Denote the channel gains from the two transmit antennas to the receive antenna as h_1 and h_2. Denote by r_{2n}

and r_{2n+1} the complex-valued signals received in two consecutive symbol periods. For $a_n = +1$, these are:

$$r_{2n} = h_1 \cdot s_{2n} - h_2 \cdot s^*_{2n+1} + \eta_{2n} \tag{38}$$

$$r_{2n+1} = h_1 \cdot s_{2n+1} + h_2 \cdot s^*_{2n} + \eta_{2n+1} \tag{39}$$

where η_{2n} and η_{2n+1} are noise components. Using (38) and (39), form the following decision variables:

$$\tilde{s}^{(+1)}_{2n} = h^*_1 \cdot r_{2n} + h_2 \cdot r^*_{2n+1} = \left(|h_1|^2 + |h_2|^2\right) s_{2n} + h^*_1 \cdot \eta_{2n} + h_2 \cdot \eta^*_{2n+1} \tag{40}$$

$$\tilde{s}^{(+1)}_{2n+1} = h^*_1 \cdot r_{2n+1} - h_2 \cdot r^*_{2n} = \left(|h_1|^2 + |h_2|^2\right) s_{2n+1} + h^*_1 \cdot \eta_{2n+1} - h_2 \cdot \eta^*_{2n} . \tag{41}$$

For $a_n = -1$, the received signals are:

$$r_{2n} = h_1 \cdot s_{2n} + h_2 \cdot s^*_{2n+1} + \eta_{2n} \tag{42}$$

$$r_{2n+1} = h_1 \cdot s_{2n+1} - h_2 \cdot s^*_{2n} + \eta_{2n+1} . \tag{43}$$

Form the following two decision variables:

$$\tilde{s}^{(-1)}_{2n} = h^*_1 \cdot r_{2n} - h_2 \cdot r^*_{2n+1} = \left(|h_1|^2 + |h_2|^2\right) s_{2n} + h^*_1 \cdot \eta_{2n} - h_2 \cdot \eta^*_{2n+1} \tag{44}$$

$$\tilde{s}^{(-1)}_{2n+1} = h^*_1 \cdot r_{2n+1} + h_2 \cdot r^*_{2n} = \left(|h_1|^2 + |h_2|^2\right) s_{2n+1} + h^*_1 \cdot \eta_{2n+1} + h_2 \cdot \eta^*_{2n} . \tag{45}$$

Suppose that a matrix with $a_n = +1$ was transmitted, but instead of (40) and (41), (44) and (45) were used. The result would be:

$$\tilde{s}^{(+1/-1)}_{2n} = \left(|h_1|^2 - |h_2|^2\right) s_{2n} - 2h^*_1 \cdot h_2 \cdot s^*_{2n+1} + h^*_1 \cdot \eta_{2n} - h_2 \cdot \eta^*_{2n+1} \tag{46}$$

$$\tilde{s}^{(+1/-1)}_{2n+1} = \left(|h_1|^2 - |h_2|^2\right) s_{2n+1} + 2h^*_1 \cdot h_2 \cdot s^*_{2n} + h^*_1 \cdot \eta_{2n+1} + h_2 \cdot \eta^*_{2n} . \tag{47}$$

On the other hand, if a matrix with $a_n = -1$ was transmitted, but instead of (44) and (45), (40) and (41) were used, the result would be:

$$\tilde{s}^{(-1/+1)}_{2n} = \left(|h_1|^2 - |h_2|^2\right) s_{2n} + 2h^*_1 \cdot h_2 \cdot s^*_{2n+1} + h^*_1 \cdot \eta_{2n} + h_2 \cdot \eta^*_{2n+1} \tag{48}$$

$$\tilde{s}^{(-1/+1)}_{2n+1} = \left(|h_1|^2 - |h_2|^2\right) s_{2n+1} - 2h^*_1 \cdot h_2 \cdot s^*_{2n} + h^*_1 \cdot \eta_{2n+1} - h_2 \cdot \eta^*_{2n} . \tag{49}$$

It is thus clear that the simple maximum likelihood decision rule proposed by Alamouti in [3] is possible only if there is certainty on the family to which the transmitted matrix belongs.

The sequence decoding of SOSTTCs is performed using the Viterbi algorithm. The observations are the complex-valued output signals of a PSK demodulator, which will be denoted as $r_{2n} = R_{2n} \cdot e^{j\varphi_{2n}}$ and $r_{2n+1} = R_{2n+1} \cdot e^{j\varphi_{2n+1}}$. Let us express the path gains from the first and the second transmit antenna to the receiver as $h_1 = H_1 \cdot e^{j\gamma_1}$ and $h_2 = H_2 \cdot e^{j\gamma_2}$. Then, for maximum likelihood sequence decoding with perfect CSI at the receiver, a suitable branch metric is given as

$$\mathrm{BM}_n = \left|r_{2n} - h_1 \cdot s_{2n} + a_n \cdot h_2 \cdot s^*_{2n+1}\right|^2 + \left|r_{2n+1} - h_1 \cdot s_{2n+1} - a_n \cdot h_2 \cdot s^*_{2n}\right|^2 . \tag{50}$$

After some simple algebra and trigonometry, we obtain:

$$\begin{aligned}\mathrm{BM}_n = {} & R^2_{2n} + R^2_{2n+1} + H^2_1 + H^2_2 \\ & - \sqrt{2} H_1 \left[R_{2n} \cdot \cos(\varphi_{2n} - \gamma_1 - k_{2n} \cdot \omega) \right. \\ & \qquad \left. + R_{2n+1} \cdot \cos(\varphi_{2n+1} - \gamma_1 - k_{2n+1} \cdot \omega)\right] \\ & + \sqrt{2} a_n \cdot H_2 \left[R_{2n} \cdot \cos(\varphi_{2n} - \gamma_2 + k_{2n+1} \cdot \omega) \right. \\ & \qquad \left. - R_{2n+1} \cdot \cos(\varphi_{2n+1} - \gamma_2 - k_{2n} \cdot \omega)\right] .\end{aligned} \tag{51}$$

The branch metric is used to reduce the number of transitions in the trellis diagram reaching the same state to a single one, called *survivor*. The branch metric with $a_n = +1$ and $a_n = -1$ is used for those transitions originating in even and odd numbered states, respectively.

When it is possible to equip the receiver with two antennas, the branch metric is simply the sum of two branch metrics as derived for a single receive antenna:

$$\mathrm{BM}_n = \mathrm{BM}^{(1)}_n + \mathrm{BM}^{(2)}_n . \tag{52}$$

The path gains are denoted by $h^{(1,q)}$ and $h^{(2,q)}$, $q = 1, 2$, for the first and the second receive antenna, respectively.

5.3 Decoding of SOSTTCs for unknown CSI at the receiver

We have two alternative strategies.

5.3.1 First decoding strategy

The first decoding strategy is essentially the method applied in [19]. Consider first a single receive antenna.

For differential decoding, the receiver is based on the following measured quantities:

$$r_{2n} = h_1 \cdot s_{2n} - h_2 \cdot a_n \cdot s^*_{2n+1} + \eta_{2n} \tag{53}$$

$$r_{2n+1} = h_1 \cdot s_{2n+1} + h_2 \cdot a_n \cdot s^*_{2n} + \eta_{2n+1} \tag{54}$$

$$r_{2n+2} = h_1 \cdot s_{2n+2} - h_2 \cdot a_{n+1} \cdot s^*_{2n+3} + \eta_{2n+2} \tag{55}$$

$$r_{2n+3} = h_1 \cdot s_{2n+3} + h_2 \cdot a_{n+1} \cdot s^*_{2n+2} + \eta_{2n+3} \tag{56}$$

where η_{2n}, η_{2n+1}, η_{2n+2}, and η_{2n+3} are noise components. The symbols r_{2n+2} in (55) and r_{2n+3} in (56) denote the complex-valued signals received in the two consecutive symbol periods $2n+2$ and $2n+3$. We need some derived quantities upon which to base our estimation on u_{2n+2} and u_{2n+3} as given in (4) and (5), respectively. Define

$$R_1 = r^*_{2n} \cdot r_{2n+2} + a_n \cdot a_{n+1} \cdot r_{2n+1} \cdot r^*_{2n+3}\,. \tag{57}$$

Introducing (52–56) in this expression, we obtain:

$$R_1 = \left(|h_1|^2 + |h_2|^2\right) u_{2n+2} + \text{noise terms}\,. \tag{58}$$

Define also

$$R_2 = r^*_{2n+1} \cdot r_{2n+2} - a_n \cdot a_{n+1} \cdot r_{2n} \cdot r^*_{2n+3}\,. \tag{59}$$

Proceeding as before, we get:

$$R_2 = \left(|h_1|^2 + |h_2|^2\right) u_{2n+3} + \text{noise terms}\,. \tag{60}$$

It is assumed that a_n is known. For both $a_{n+1} = +1$ and $a_{n+1} = -1$, the receiver computes the closest vector $(u_{2n+2}\ u_{2n+3})$ to $(R_1\ R_2)$. If hard decision is used, by inverse mapping, the bits used further in the Viterbi algorithm are obtained. However, if soft decision is applied, the quantized version of $(R_1\ R_2)$ is used in the Viterbi algorithm.

When the receiver is equipped with two antennas, using the same method, we compute $R_1^{(1)}$ and $R_2^{(1)}$ for the first antenna and $R_1^{(2)}$ and $R_2^{(2)}$ for the second antenna. Then, the closest vector $(u_{2n+2}\ u_{2n+3})$ to $(R_1^{(1)} + R_1^{(2)}\ \ R_2^{(1)} + R_2^{(2)})$ is computed. The rest of the procedure is the same as explained for a single receive antenna.

5.3.2 Second decoding strategy

The transmission matrix at the discrete time $n+1$, according to (2), is:

$$\mathbf{M}_{n+1} = \begin{pmatrix} s_{2n+2} & -a_{n+1} \cdot s^*_{sn+3} \\ s_{2n+3} & a_{n+1} \cdot s^*_{sn+2} \end{pmatrix}. \tag{61}$$

We can write the branch metric as

$$\begin{aligned} \text{BM}_{n+1} = &\left| r_{2n+2} - h_1 \cdot s_{2n+2} + h_2 \cdot s^*_{2n+3} \right|^2 \\ &+ \left| r_{2n+3} - h_1 \cdot s_{2n+3} - h_2 \cdot s^*_{2n+2} \right|^2 . \end{aligned} \tag{62}$$

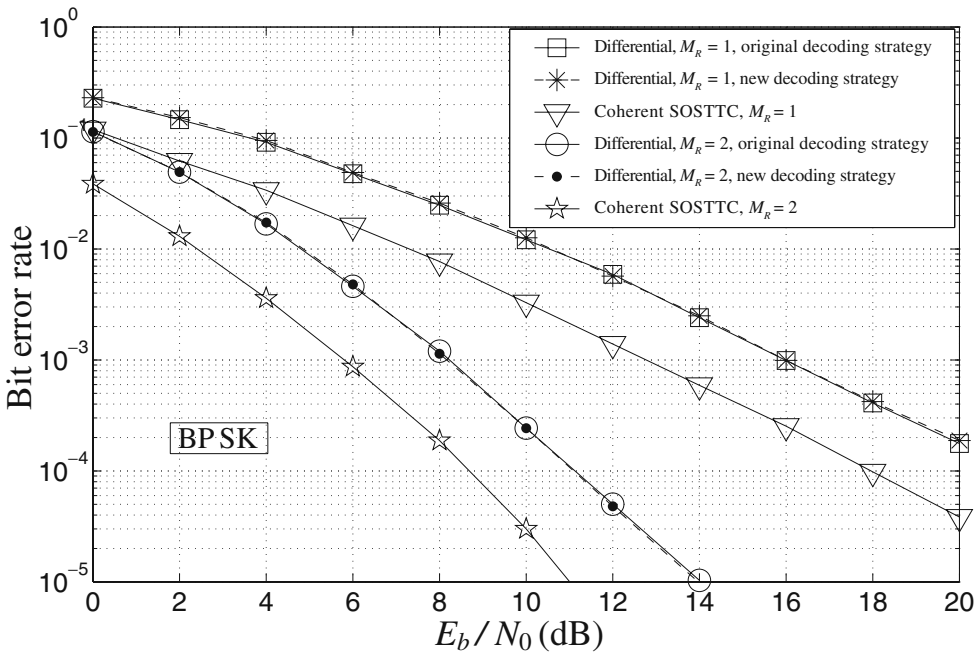

Fig. 8 Performance of differential SOSTTC and coherent SOSTTC BPSK for one ($M_R = 1$) receive antenna and two ($M_R = 2$) antennas

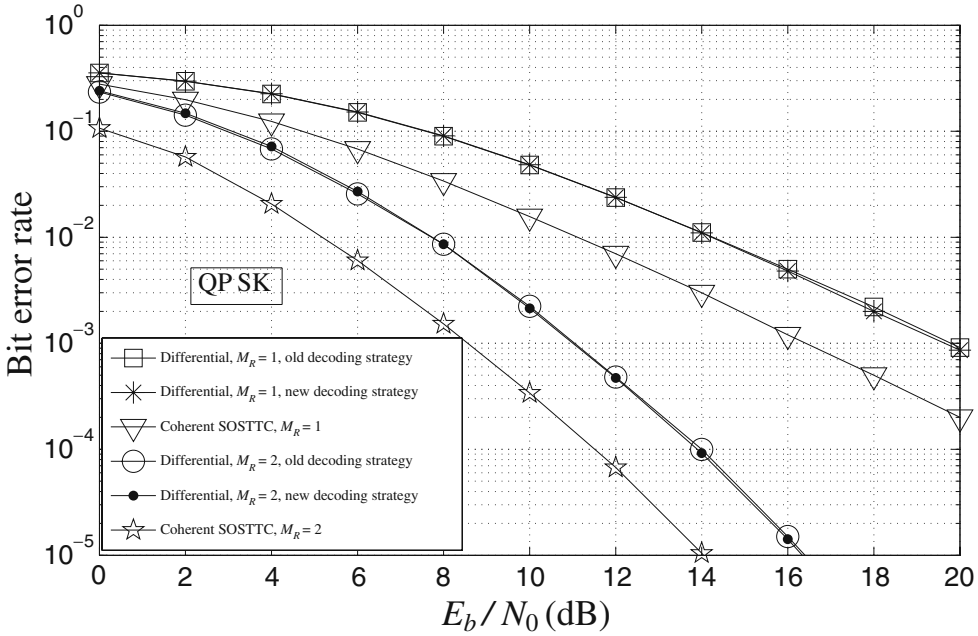

Fig. 9 Performance of differential SOSTTC and coherent SOSTTC QPSK for one ($M_R = 1$) receive antenna and two ($M_R = 2$) antennas

From (62), we obtain:

$$\begin{aligned}\mathrm{BM}_{n+1} = {} & |r_{2n+2}|^2 + |r_{2n+3}|^2 + \left(|h_1|^2 + |h_2|^2\right) \\ & \times \left(\left|s_{2n+2}^2\right|^2 + \left|s_{2n+3}^2\right|^2\right) \\ & + 2\mathrm{Re}\left\{r_{2n+2}\left(-h_1^* \cdot s_{2n+2}^* + h_2^* \cdot a_{n+1} \cdot s_{2n+3}\right)\right. \\ & \left. + r_{2n+3}\left(-h_1^* \cdot s_{2n+3}^* - h_2^* \cdot a_{n+1} \cdot s_{2n+2}\right)\right\}. \end{aligned} \tag{63}$$

The first terms are positive and common to all state transitions of a trellis section. Only the last term depends on the signal being actually transmitted. Define thus the reduced metric

$$\begin{aligned}\mathrm{RM}_{n+1} = {} & 2\mathrm{Re}\left\{r_{2n+2}\left(-h_1^* \cdot s_{2n+2}^* + h_2^* \cdot a_{n+1} \cdot s_{2n+3}\right)\right. \\ & \left. + r_{2n+3}\left(-h_1^* \cdot s_{2n+3}^* - h_2^* \cdot a_{n+1} \cdot s_{2n+2}\right)\right\}. \end{aligned} \tag{64}$$

The branch metric BM_{n+1} is minimized by the most negative value of the reduced metric RM_{n+1}. Using the

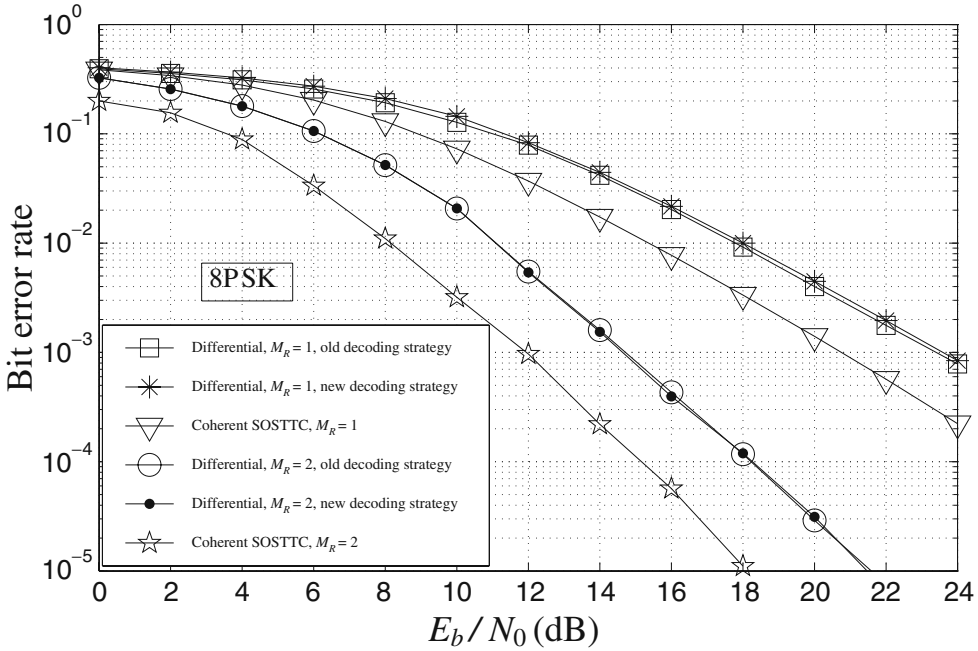

Fig. 10 Performance of differential SOSTTC and coherent SOSTTC 8PSK for one ($M_R = 1$) receive antenna and two ($M_R = 2$) antennas

differential encoding, we have:

$$\begin{aligned}\mathrm{RM}_{n+1} = 2\mathrm{Re}\{&u_{2n+2}\left[r^*_{2n+2}\left(-h_1\cdot s_{2n}+h_2\cdot a_n\cdot s^*_{2n+1}\right)\right]\\&+r_{2n+3}\left(-h^*_1\cdot a_n\cdot s^*_{2n+1}-h^*_2\cdot s_{2n}\right)a_{n+1}\Big]\\&+u_{2n+3}\left[r^*_{2n+2}\left(-h_1\cdot s_{2n+1}-h_2\cdot a_n\cdot s^*_{2n}\right)\right.\\&\left.+r_{2n+3}\left(h^*_1\cdot a_n\cdot s^*_{2n}-h^*_2\cdot s_{2n+1}\right)\right.\\&\left.\times a_{n+1}\right]\Big\}. \qquad (65)\end{aligned}$$

By neglecting the noise term, we can write:

$$r_{2n} = h_1\cdot s_{2n} - h_2\cdot a_n\cdot s^*_{2n+1} \qquad (66)$$

$$r_{2n+1} = h_1\cdot s_{2n+1} + h_2\cdot a_n\cdot s^*_{2n}. \qquad (67)$$

Finally, we obtain:

$$\begin{aligned}\mathrm{RM}_{n+1} = -2\mathrm{Re}\{&\left(r_{2n}\cdot r^*_{2n+2}+a_n\cdot a_{n+1}\cdot r^*_{2n+1}\cdot r_{2n+3}\right)u_{2n+2}\\&+\left(r_{2n+1}\cdot r^*_{2n+2}-a_n\cdot a_{n+1}\cdot r^*_{2n}\cdot r_{2n+3}\right)u_{2n+3}\Big\}.\end{aligned} \qquad (68)$$

For each state transition, the receiver knows all the quantities from this expression. The survivor is selected as that transition entering a given next state that makes RM_{n+1} to be the most negative one. The knowledge of h_1 and h_2 is obviously not required.

6 Simulation results

In this section, we first compare the performance of the differential SOSTTCs decoded by the two algorithms described in Section 5. All the three signal constellations, i.e. BPSK, QPSK and 8PSK, have been considered. For comparison, we also present simulation results for SOSTTCs using the coherent encoding scheme. Moreover, we study the effect of the antenna spacing and the angular spread of scatterers on the BER performance of the differential SOSTTCs.

In all simulations, the AODs and the AOAs were determined by using the MMEA with $M_s = 40$ and $N_s = 50$, $\beta_T = \beta_R = \pi/2$ and $\phi_T^{\max} = \phi_R^{\max} = 2°$. The transmitter and the receiver moved in the direction determined by the angles of motion $\alpha_T = 60°$ and $\alpha_R = 60°$. The maximum Doppler frequencies at both sides were equal to 91 Hz. The chosen value 91 Hz is for the case when the carrier frequency is 900 MHz and the speed of the mobile unit is 110 km/h. If not mentioned otherwise, we assume that the scatterers were located uniformly on the two rings, i.e. the parameter κ controlling the angular spread in the von Mises distribution equals zero.

The performance comparison between the differential SOSTTCs using the proposed decoding algorithm and the conventional decoding algorithm is depicted in Fig. 8 for BPSK. The comparison between the two aforementioned decoding algorithms is presented in Fig. 9 for QPSK and in Fig. 10 for 8PSK. In these three figures, we also present the simulation results for the cases in which the receiver is equipped with one antenna and two antennas. It is seen from Figs. 8–10 that the proposed algorithm has the same decoding performance as the conventional algorithm. For the sake of comparison, Figs. 8–10 also present the BER performance of the coherent SOSTTC. It can be concluded from the three figures that a loss of 3 dB occurs when differential SOSTTCs are used instead of coherent SOSTTCs, what fully agrees with [19].

In addition, we compare the simulation time of the differential SOSTTCs using both decoding algorithms for the case $M_T = 2$ and $M_R = 1$. The Tables 4, 5, and 6 show the simulation time required for the differential SOSTTC using the BPSK, QPSK and 8PSK constellation, respectively. The quantity L in these three tables denotes the number of symbols used in the simulation runs. According to Tables 4–6, we find that, for the differential BPSK, QPSK and 8PSK scheme, the simulation time using the new decoding algorithm is approximately 70%, 68% and 58% of that using the traditional one, from which we may conclude that the proposed decoding algorithm has a lower complexity. Moreover, the new decoding algorithm works more

Table 5 Comparison of the required simulation time for the QPSK constellation

Strategy	Number of symbols L			
	10^4	10^5	10^6	10^7
Traditional decoding strategy (s)	1.75	16.62	165.66	1,651.60
New decoding strategy (s)	1.30	11.24	112.50	1,125.41

Table 4 Comparison of the required simulation time for the BPSK constellation

Strategy	Number of symbols L			
	10^4	10^5	10^6	10^7
Traditional decoding strategy (s)	0.80	7.92	78.84	792.98
New decoding strategy (s)	0.61	5.54	55.52	554.13

Table 6 Comparison of the required simulation time for the 8PSK constellation

Strategy	Number of symbols L			
	10^4	10^5	10^6	10^7
Traditional decoding strategy (s)	4.63	45.87	459.68	4,546.00
New decoding strategy (s)	2.71	26.56	260.38	2,643.62

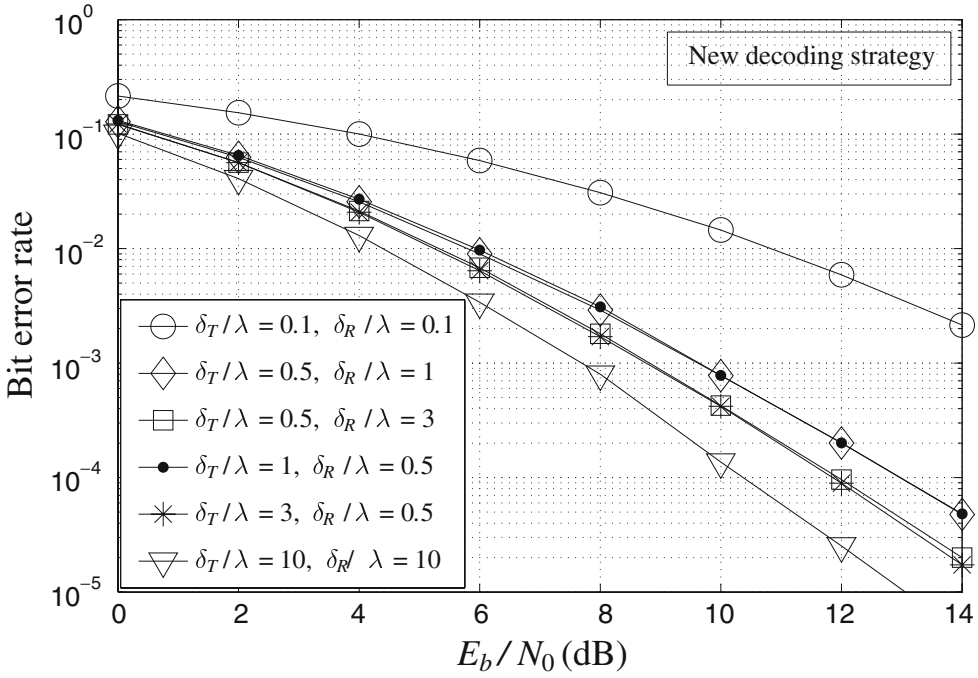

Fig. 11 The effect of the antenna spacings on the BER performance of differential BPSK SOSTTC under isotropic scattering conditions ($\kappa = 0$, $M_T = 2$, $M_R = 2$)

efficiently for differential SOSTTCs having a larger size of signal constellation.

In the following, we study the effect of the antenna spacing and the angular spread of the incoming waves on the performance of the differential SOSTTC with BPSK. Here, we only focus on the differential SOSTTC using the new decoding algorithm. Moreover, we assume that the transmitter and the receiver are equipped with two antennas.

Figure 11 illustrates the impact of the antenna spacing on the BER performance. As expected, the BER performance improves with increasing antenna spacings,

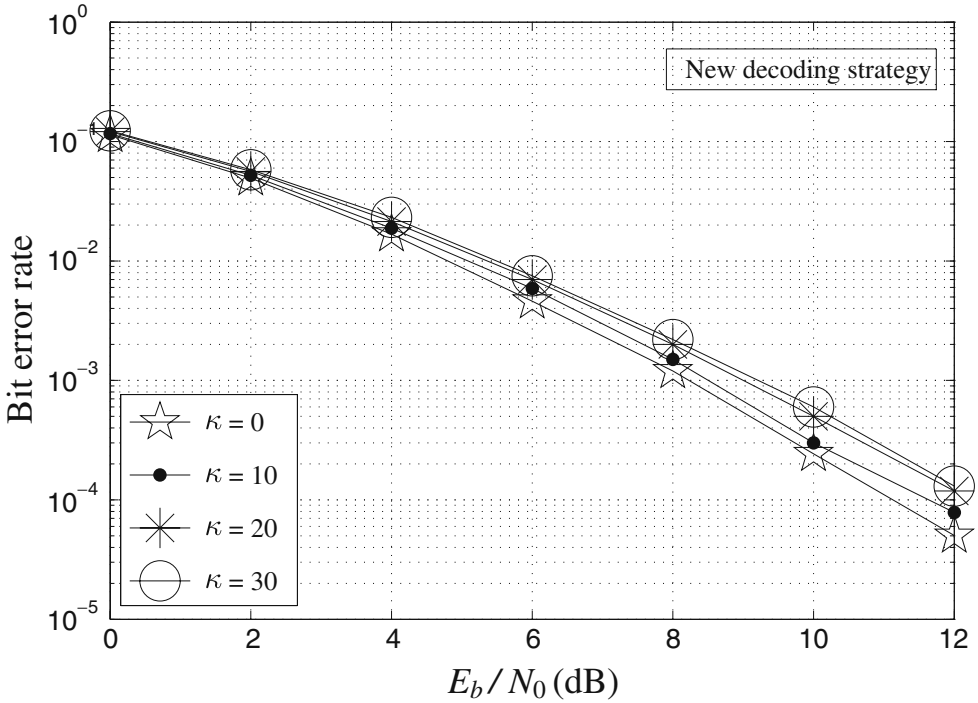

Fig. 12 The effect of the angular spread ($\approx 2/\sqrt{\kappa}$) on the BER performance of differential BPSK SOSTTC under isotropic ($\kappa = 0$) and nonisotropic ($\kappa \neq 0$) scattering conditions ($\delta_T = 10\lambda$, $\delta_R = 3\lambda$, $M_T = 2$, $M_R = 2$)

while the performance deteriorates if the antennas become close to each other. The reason for this behavior is that the spatial correlation between the channel gains decreases as the antenna spacing becomes larger. It seems that the transmitter and the receiver have almost equivalent influence on the BER performance. This can be explained on account of the symmetry of the geometrical two-ring scattering model and the equal values set for the main parameters of the transmitter and the receiver.

Figure 12 shows the impact of the angular spread of the incoming waves on the BER performance. The considered propagation scenarios include both isotropic ($\kappa = 0$) and nonisotropic ($\kappa \neq 0$) scattering. In simulations, we assume that the scatterers are clustered around the mean AOA $\mu = \pi$ and the antenna spacings are fixed to $\delta_T = 10\lambda$ and $\delta_R = 3\lambda$. It is shown that increasing the value of κ leads to performance degradations. However, when the scatterers are highly centralized, e.g. when $\kappa = 20$, no significant performance difference can be observed if we further increase the value of κ.

7 Conclusions

In this paper, a differential encoding scheme has been applied to design new and better SOSTTCs for noncoherent mobile communication systems for which CSI is not available at both the transmitter and the receiver. A two-ring MIMO channel simulator has been used to study the performance of the differential SOSTTCs for BPSK, QPSK and 8PSK. Moreover, we have proposed a new decoding algorithm. It has been shown by simulations that the proposed decoding algorithm can provide the same performance compared with the traditional strategy, while it reduces the decoding complexity by approximately 30%. The proposed decoding algorithm works more efficiently for a larger size of signal constellation. For example, for differential 8PSK scheme, the new algorithm can save around 42% decoding time compared with the traditional algorithm. Our simulations have confirmed the engineering intuition that the system performance depends greatly on the antenna spacing as well as on the angular spread of the incoming waves. Moreover, we have compared the BER performance of the differential SOSTTCs with that of the coherent SOSTTCs. As expected, the coherent scheme outperforms the differential one by a coding gain of approximately 3 dB.

References

1. Abdi A, Barger JA, Kaveh M (2002) A parametric model for the distribution of the angle of arrival and the associated correlation function and power spectrum at the mobile station. IEEE Trans Veh Technol 51(3):425–434
2. Agrawal D, Richardson TL, Urbanke RL (2001) Multiple-antenna signal constellations for fading channels. IEEE Trans Inf Theory 47(6):2618–2626
3. Alamouti SM (1998) A simple transmit diversity technique for wireless communications. IEEE J Sel Areas Commun 16(8):1451–1458
4. Bahceci I, Duman TM (2004) Trellis-coded unitary space-time modulation. IEEE Trans Wirel Commun 3(6):2005–2012
5. Edbauer F (1989) Performance of interleaved trellis-coded differential 8-PSK modulation over fading channels. IEEE J Sel Areas Commun 7:1340–1346
6. Gutiérrez CA, Pätzold M (2007) Sum-of-sinusoids-based simulation of flat fading wireless propagation channels under non-isotropic scattering conditions. In: Proc 50th IEEE global communications conference, IEEE GLOBECOM 2007, Washington DC, USA, pp 3842–3846
7. Hochwald BM, Marzetta TL (2000) Unitary space-time modulation for multiple-antenna communications in Rayleigh flat fading. IEEE Trans Inf Theory 46:543–564
8. Hochwald BM, Marzetta TL, Richardson TJ, Sweldens W, Urbanke R (2000) Systematic design of unitary space-time constellations. IEEE Trans Inf Theory 46(6):1962–1973
9. Hughes BL (2000) Differential space-time modulation. IEEE Trans Inf Theory 46:2567–2578
10. Jafarkhani H, Seshadri N (2003) Super-orthogonal space-time trellis codes. IEEE Trans Inf Theory 49:937–950
11. Jafarkhani H, Tarokh V (2001) Multiple transmit antenna differential detection from generalized orthogonal designs. IEEE Trans Inf Theory 47(6):2626–2631
12. Ma Y, Pätzold M (2007) Wideband two-ring MIMO channel models for mobile-to-mobile communications. In: Proc 10th international symposium on Wireless Personal Multimedia Communications, WPMC 2007, Jaipur, India, pp 380–384
13. McLane PJ et al (1988) PSK and DPSK trellis codes for fast fading, shadowed mobile satellite communication channels. IEEE Trans Commun 36:1242–1246
14. Schlegel C, Costello DJ Jr (1989) Bandwidth efficient coding for fading channels: code construction and performance analysis. IEEE J Sel Areas Commun 7:1356–1368
15. Sterian CED, Enescu AA, Bănică I (2007) Super-orthogonal space-time trellis codes with eight dimensional phase-shift keying signal constellations. Ann Télécommun 62(3/4):486–512
16. Sun Z, Tjhung TT (2003) On the performance analysis and design criteria for trellis coded unitary space-time modulation. IEEE Commun Lett 7(4):156–158
17. Sun Z, Tjhung TT (2004) Multiple-trellis-coded unitary space-time modulation in Rayleigh flat fading. IEEE Trans Wirel Commun 3(6):2335–2334
18. Tao M, Cheng RS (2003) Trellis-coded differential unitary space-time modulation over flat fading channels. IEEE Trans Commun 51(4):587–596

19. Tarokh V, Jafarkhani H (2000) A differential detection scheme for transmit diversity. IEEE J Sel Areas Commun 18(7):1169–1174
20. Tarokh V, Seshadri N, Calderbank AR (1998) Space-time codes for high data rate wireless communication: performance criterion and code construction. IEEE Trans Inf Theory 44(2):744–765
21. Ungerboeck G (1982) Channel coding with multilevel/phase signals. IEEE Trans Inf Theory IT-28:55–67
22. Wei LF (1984) Rotationally invariant convolutional channel coding with expanded signal space - part I: 180° and part II: nonlinear codes. IEEE J Sel Areas Commun 2:659–686
23. Wei LF (1993) Coded M-PSK with built-in time diversity for fading channels. IEEE Trans Inf Theory 39(6):1820–1839
24. Wu Y, Lau VKN, Pätzold M (2006) Constellation design for trellis-coded unitary space-time modulation systems. IEEE Trans Commun 54(11):1948–1959
25. Zhao W, Leus G, Giannakis GB (2004) Orthogonal design of unitary constellations for uncoded and trellis-coded noncoherent space-time systems. IEEE Trans Inf Theory 50(6):1319–1327
26. Zhu Y, Jafarkhani H (2006) Differential super-orthogonal space-time trellis codes. IEEE Trans Wirel Commun 5(12):3634–3643